JM PAPERS

On the physical nature of the turbulent/turbulent interface

Krishna S. Kankanwadi[1] and **Oliver R.H. Buxton**[1,†]

[1]Department of Aeronautics, Imperial College London, South Kensington Campus, London SW7 2AZ, UK

The existence of a turbulent/turbulent interface (TTI) has recently been verified in the far wake of a circular cylinder exposed to free-stream turbulence (Kankanwadi & Buxton, *J. Fluid Mech.*, vol. 905, 2020, p. A35). This study aims to understand the physics within the TTI. The wake boundary, approximately 40 diameters downstream of a circular cylinder subjected to grid-generated turbulence, was investigated through simultaneous cinematographic, stereoscopic particle image velocimetry and planar laser induced fluorescence experiments. With no grid placed upstream of the cylinder, the behaviour of the resultant interface, our closest approximation to a turbulent/non-turbulent interface, exactly matched what is observed in existing literature. When background turbulence is present, viscous action is no longer the only method by which enstrophy is transported to the background fluid, unlike for turbulent/non-turbulent interfaces. The presence of rotational fluid on both sides of the TTI allows the vorticity stretching term of the enstrophy budget equation to be the dominant actor in this process. The role of viscosity within a TTI is greatly diminished as the vorticity stretching term takes over responsibilities for enstrophy production. The turbulent strain rate normal to the TTI was found to be enhanced in the interfacial region. Decomposing the vorticity stretching term into components aligned with the three principal strain-rate directions, it was found that the term most aligned with the interface-normal direction contributed to the largest share of enstrophy production. This indicates that better 'organised' vorticity on the wake side of the interface yields the enstrophy amplification leading to the previously discovered enstrophy jump across the TTI by Kankanwadi & Buxton (*J. Fluid Mech.*, vol. 905, 2020, p. A35).

Key words: wakes, turbulent mixing

† Email address for correspondence: o.buxton@imperial.ac.uk

1. Introduction

The spatio-temporal processes by which turbulent bodies of fluid expand into the background fluid, such as the growth of a volcanic plume into the atmosphere with distance from the crater, are collectively known as entrainment. These entrainment processes are critical in defining the behaviour of numerous industrial and environmental phenomena. These range from the design of wind farms to the governance of meteorological phenomena such as cloud formation in both terrestrial and extra-terrestrial settings (Atreya *et al.* 1999; de Rooy *et al.* 2013). The rate and process by which this entrainment occurs is governed by small-scale turbulent dynamics within an interfacial layer adjacent to the outermost boundary between the two regions of fluid. In the special case where the background fluid is non-turbulent this layer is known as the turbulent/non-turbulent interface (TNTI).

The nature of the TNTI is best explained by examining the behaviour of the terms of the enstrophy budget equation

$$\frac{D}{Dt}\frac{\omega^2}{2} = \underbrace{\omega_i\omega_j s_{ij}}_{\text{vorticity stretching}} + \underbrace{\nu\frac{\partial^2(\omega^2/2)}{\partial x_j \partial x_j}}_{\text{viscous diffusion}} - \underbrace{\nu\left(\frac{\partial \omega_i}{\partial x_j}\right)^2}_{\text{viscous dissipation}}. \tag{1.1}$$

A key distinguishing feature of turbulent flow is that it is vortical, i.e. $\omega^2 = |\nabla \times \boldsymbol{u}|^2 \neq 0$, where $\boldsymbol{u}(\boldsymbol{x})$ is the velocity field and $\boldsymbol{\omega}$ is the vorticity, whereas non-turbulent flow is usually irrotational, $\omega^2 = 0$. Accordingly, the outermost boundary between the turbulent and non-turbulent fluid, the irrotational boundary, is an isosurface of $\omega^2 = 0$. Corrsin & Kistler (1955) thereby first postulated the existence of a viscous superlayer at the outer edge of the TNTI. They argued that inside the superlayer the viscous diffusion term of the enstrophy budget equation, $\nu(\partial^2(\omega^2/2)/\partial x_j \partial x_j)$, solely dominates and, hence, viscosity takes complete responsibility for enstrophy ($\omega^2/2$) production and facilitates the transfer of vortical motions to the surrounding fluid. This is necessitated by the fact that $\omega^2 = 0$ at the irrotational boundary ensuring that the vorticity stretching term $\omega_i\omega_j s_{ij}$ must drop to zero here. The action of viscosity thus remains the only method by which vorticity may be transferred to the irrotational background, thereby growing the turbulent flow via entrainment.

Using dimensional arguments, Corrsin & Kistler (1955) further deduced that the thickness of this layer, where vorticity is diffused into the surrounding fluid, must scale with the Kolmogorov length scale and, furthermore, the defining velocity scale in this region is the Kolmogorov velocity scale. Here the Kolmogorov length η and velocity u_η scales characterise the smallest, dissipative motions in turbulence and are formed from the rate of dissipation of turbulent kinetic energy per unit mass ε and kinematic viscosity of the fluid ν, i.e. $\eta = (\nu^3/\varepsilon)^{1/4}$ and $u_\eta = (\nu\varepsilon)^{1/4}$. Many years later, these scalings were experimentally verified by Holzner *et al.* (2007).

The TNTI is considered to encompass the layer of fluid in which the enstrophy adjusts from zero, in the background, to the bulk value within the turbulent flow in a conditional mean sense. Many subsequent studies have shown the TNTI to be substantially thicker than simply the viscous superlayer (Van Reeuwijk & Holzner 2013; da Silva *et al.* 2014). Once the enstrophy level within the TNTI becomes non-negligible the vorticity stretching term $\omega_i\omega_j s_{ij}$ takes over as the dominant source of enstrophy production (da Silva *et al.* 2014; Watanabe *et al.* 2014). Van Reeuwijk & Holzner (2013) coined this region of the TNTI the turbulent buffer layer and defined the thickness of the viscous superlayer to be

the point at which the enstrophy production via viscous diffusion decays to insignificance. Throughout the TNTI the viscous dissipation acts as a constant sink of enstrophy.

Whilst the behaviour of these terms and their contribution to turbulent entrainment is well established for a TNTI, an understanding of the mechanisms of entrainment is lacking when rotational fluid is present on both sides of the bounding interface, despite the fact that the majority of environmental and industrial flows occur within a turbulent background. For example, in our volcanic plume example the atmospheric boundary layer ensures that the background fluid is itself turbulent. Few studies have examined entrainment from a turbulent background but those that have highlighted the effect of both the characteristic length scale and intensity of the background turbulence without definitively ascertaining the relative importance of both (Ching, Fernando & Robles 1995; Gaskin, McKernan & Xue 2004; Eames, Jonsson & Johnson 2011). Kankanwadi & Buxton (2020) conducted a parametric study and concluded that background turbulence intensity is the defining feature whereas the length scale only has a second-order effect in the far wake of a cylinder exposed to free-stream turbulence. However, the literature is scarce and the physics of the turbulent/turbulent interface (TTI), henceforth defined analogously to the TNTI as the region of fluid immediately adjacent to the outermost boundary of the primary turbulent flow, are as yet unknown. Indeed, in the review paper of da Silva *et al.* (2014) it was suggested that TTIs cease to exist when the intensity of the turbulence within the bulk flow and the background turbulence are comparable to one another.

This gap in the knowledge has left behind some profound questions which we aim to address in this paper. This paper builds on the work reported in Kankanwadi & Buxton (2020) and aims to investigate the physics of the TTI. Firstly, the crucial result that confirms the existence of the TTI is reproduced in this paper to aid the narrative. Following on from this we seek to identify the important flow physics at the boundary between the wake and the turbulent background. In the case of turbulent/turbulent entrainment the phenomenology as described by Corrsin & Kistler (1955) is no longer applicable, since a TTI is unlikely to be an isosurface of $\omega^2 = 0$ and, hence, all three source terms on the right-hand side of (1.1) are likely to be non-zero, including the vorticity stretching term. Answering these questions is vital to more accurately modelling turbulent flows spreading into a turbulent background since existing modelling strategies are often based around the assumption that diffusion plays the dominant role.

2. Methodology

In a similar vein to the study of Kankanwadi & Buxton (2020), a parametric study has been conducted on the far wake of a circular cylinder that is subjected to cases of grid-generated background turbulence, in which the length scale L_{12} and intensity *TI* of the background turbulence can be independently controlled. Simultaneous, cinematographic stereoscopic particle image velocimetry (PIV) (Ganapathisubramani, Lakshminarasimhan & Clemens 2007) and planar laser induced fluorescence experiments (PLIF) were conducted approximately 40 diameters downstream of the rear face of the circular cylinder. In order to asses the entrainment mechanisms within the TTI, all three components of velocity as well as all nine components of the velocity gradient tensor were required. This was achieved by invoking Taylor's hypothesis between consecutive stereoscopic PIV velocity fields to produce an instantaneous quasi-three-dimensional, three component (of the velocity vector) data set. The in-plane velocity gradients could be readily calculated using the stereoscopic PIV data. Streamwise velocity gradients were extracted after
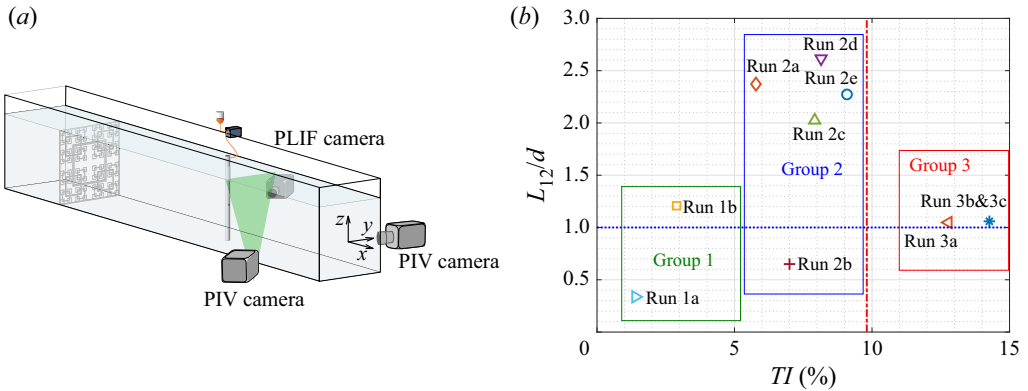
(*a*)

Figure 1. (*a*) An illustration of the experimental set-up. Note that the laboratory coordinate system has been shifted downstream in the interest of clarity. (*b*) Experimental envelope of the campaign highlighting the background turbulence parameters for all conducted runs. Note that the blue dotted line represents a value equal to one cylinder diameter. The red dot-dashed line indicates the turbulence intensity found inside the wake for the no-gird case at the location of the field of view (Kankanwadi & Buxton 2020).

invoking Taylor's hypothesis. These experiments were conducted in a water facility at Imperial College London at a Reynolds number with respect to the cylinder diameter of approximately 4000. In our interrogated field of view the local turbulent Reynolds number, based on the Taylor length scale and r.m.s. velocity fluctuation, was $Re_\lambda = 94$. In order to examine the interface it is necessary for the experimental set-up to achieve a near Kolmogorov-scale spatial resolution. A combination of a 12 mm extension tube mounted onto a Nikkor 200 mm lens was utilised to achieve a spatial resolution of approximately 3.6η which is comparable to direct numerical simulation (DNS) resolution. An illustration of the set-up used in the experimental campaign is depicted in figure 1(*a*). Note that the origin of the laboratory coordinate system depicted in the figure has been shifted downstream of the rear face of the cylinder, where it should lie, in the interest of clarity. Figure 1(*b*) outlines the parametric envelope of this campaign. The background turbulence parameters present at the location of the field of view are highlighted in the figure along with lines indicating the cylinder diameter as well as the turbulence intensity found inside the wake for the no-grid (virtually non-turbulent) background conditions. These runs are split into three groups based mainly on the background turbulence intensity but also as a result of the displayed entrainment behaviour highlighted by Kankanwadi & Buxton (2020). Runs in group 1 are most similar to the no-grid case whereas group 3 classifies runs where the intensity of the background turbulence is so extreme that it is larger than the intensity within the wake itself. Within each group the runs are further named in hierarchical order based on the intensity of the incoming background turbulence. This classification is reflected in the naming convention with the numerical prefix representing the group (run #*x*) whereas the hierarchical order within each group is represented by the suffix in the form of the Latin alphabet in ascending order (run #*x*).

Having access to simultaneous PLIF data is necessary in order to demarcate the wake from the free stream. Using classical methods to identify TNTIs, such as using vorticity magnitude or turbulent kinetic energy thresholds, is not viable since rotational/turbulent fluid is available on both sides of the interface. Instead, a high-Schmidt-number scalar in the form of Rhodamine 6G is released from the rear face of the cylinder. A high Schmidt number ensures that molecular diffusion occurs over a vanishingly small length

scale and, hence, the scalar acts as a faithful fluid marker. The scalar is well mixed and covers the full extent of the wake in the immediate vicinity downstream of the cylinder (Kankanwadi & Buxton 2020). This allows the PLIF camera, focused on the wake downstream, to successfully capture the location of the wake boundary. The camera is fitted with a low-pass filter to exploit the shifted emission peak of Rhodamine 6G in order to only capture the tracer data whilst ignoring light scattered by the PIV seeding particles. Interface identification is then performed on images of the dye by placing a threshold on the modulus of the captured light intensity gradient, $|\nabla \phi|$. A similar strategy was used in Kankanwadi & Buxton (2020) and was shown to work effectively in measuring entrainment into a turbulent wake exposed to a turbulent background (instantaneously capturing both entrainment and detrainment).

Prior to addressing the results, it is important to highlight that due to the geometry of the experimental set-up, some slight smearing of the statistics exists in the presented results. The light sheet thickness causes a small, yet finite volume to be illuminated in the region of interest. The PLIF image captured is thereby a line of sight integration over the light sheet thickness. This may lead to situations where the extracted scalar extent could sit some small distance from the true wake boundary potentially introducing some smearing of the statistics. However, it is important to highlight that in spite of these issues with the nature of the experiment, the physics in the interfacial region have been captured and match similar results in literature that have been obtained using DNS. Further evidence for this is provided in § 4.

As with any experimentally obtained data set for an incompressible flow, a non-zero divergence error, i.e. $\nabla \cdot \boldsymbol{u} \neq 0$, exists within the raw data due to the presence of measurement noise. A divergence correction scheme as laid out by de Silva, Philip & Marusic (2013) was implemented with a threshold on the magnitude of the divergence error of 10 s^{-1}. The scheme was successful in significantly reducing the divergence error whilst ensuring that the magnitude of the 'correction noise' added to the data set was below 1 % of the mean free-stream velocity, i.e. to within the existing experimental uncertainty. All of the results presented in this paper have been calculated using data sets that have been corrected for divergence error.

3. Turbulent/turbulent interface

Prior to addressing the mechanisms of entrainment it is imperative to address the zeroth-order question of whether a TTI even exists, which has been previously questioned (e.g. da Silva *et al.* 2014). Results relating to this question were first reported in Kankanwadi & Buxton (2020) and are reproduced in this paper in the form of figure 2. The figure plots the behaviour of conditional mean enstrophy as a function of normal distance away from the outer wake boundary γ for several runs with varying background turbulence intensities and length scales. It is clear to see that even in the presence of background turbulence an enstrophy jump (reminiscent of TNTIs, e.g. Bisset, Hunt & Rogers (2002), Westerweel *et al.* (2005) etc.) is reproduced, holding true even in the most extreme background turbulence characteristics that are found in group 3 cases. This enstrophy jump represents a discontinuity in flow properties between the wake and the background independently of the (artificially introduced) passive scalar.

The two-point statistics of the interfacial region may be examined by means of interface-normal correlation functions in the vicinity of the wake boundary. Figure 3 depicts the correlation of the fluctuating spanwise component of vorticity in the
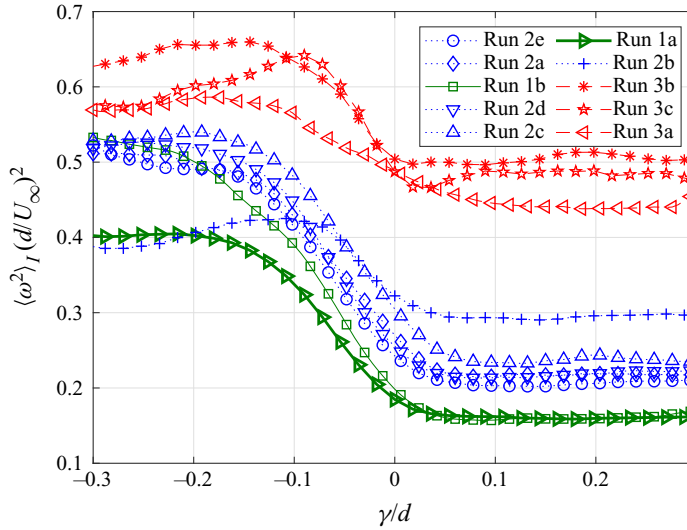
Figure 2. Mean enstrophy as a function of normal distance away from the interface (Kankanwadi & Buxton 2020).

interface-normal direction, $R_{\omega_3'\gamma}$,

$$R_{\omega_3'\gamma} = \frac{\langle \omega_3'(\gamma)\omega_3'(\gamma + r)\rangle}{\sqrt{\langle \omega_3'^2(\gamma)\rangle}\sqrt{\langle \omega_3'^2(\gamma + r)\rangle}}. \tag{3.1}$$

The fixed probe is located $0.05d$ into the free-stream side of the boundary, i.e. $\gamma = 0.05d$, and r denotes the distance from the fixed probe to the moving probe in the interface-normal direction. Solid lines in the figure represent correlations in which r points in the direction of the wake, whereas dashed lines indicate r pointing into the free stream. In the interest of clarity only one example from each group has been presented in figure 3. As expected, an asymmetric correlation function is observed with a more rapid decorrelation witnessed as the moving probe crosses the wake boundary (solid lines), in comparison to a slower decorrelation as the moving probe traverses the free stream (dashed lines). The level of asymmetry between the correlation functions pointing in different directions relative to the interface is seen to drop for cases with increased background turbulence intensity; however, this may be expected since more intense turbulence is expected to decorrelate over a physically shorter distance. We thus confirm there exists a TTI where the enstrophy adjusts itself between the levels found on either side of the interface, similarly to the TNTI. We finish by drawing an analogy between the TTI and internal shear layers (across which there is a discontinuity in, and decorrelation of, turbulent statistics) which are thought to be a feature of homogeneous, high-Reynolds-number turbulence (Hunt *et al.* 2010; Ishihara, Kaneda & Hunt 2013). Such high-Reynolds-number turbulence displays strong intermittency at small scales and is ubiquitous in nature, governing processes such as meteorology or magneto-hydrodynamics.

Whilst, it is not the intention of this paper to establish a scaling for the identified TTI thickness, it can be useful to represent the thickness of the interface as a function of known turbulent length scales. The vorticity adjustment region of run 1a (our closest approximation to a TNTI) may be estimated to have a thickness of $0.2d$. Using the Taylor
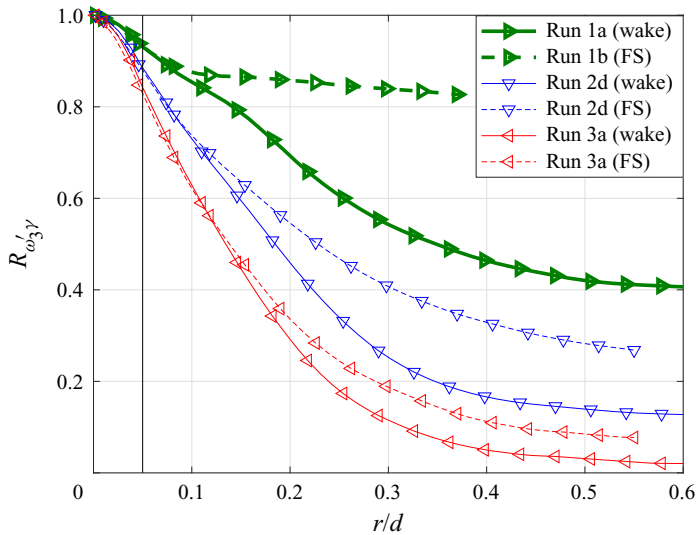
Figure 3. Correlation function of the fluctuating spanwise vorticity component, ω'_3, in the interface-normal direction. Note that the probe is placed at $\gamma = 0.05d$. The solid lines depict the boundary normal direction pointed into the wake, whereas the dashed lines represent the direction pointed into the free stream (FS). The vertical solid line represents the position of the wake boundary relative to the probe for the correlations pointed towards the wake (solid lines).

and Kolmogorov scale calculated for the no-grid case, $0.2d$ is equivalent to approximately 0.7λ and 12.5η. These are in line with the TNTI thicknesses observed in the literature (e.g. Silva, Zecchetto & Da Silva 2018). We also note that the solid and dashed correlations of figure 3, i.e. those pointing towards the wake and the free stream, begin to diverge at $r \approx 0.12d$, i.e. $\approx 0.07d$ into the interface. This corresponds to $\approx 4.5\eta$, which is very close to the widely accepted thickness for the viscous superlayer of a TNTI, although we make no claims as to having identified the viscous superlayer thickness from these correlation functions.

4. Flow physics within the TTI

The TTI is now investigated through the lens of the enstrophy budget equation (1.1) to ascertain the relevant flow physics. Analysis of this manner for TNTIs can be found in previous literature (e.g. Van Reeuwijk & Holzner 2013; Silva *et al.* 2018; Buxton, Breda & Dhall 2019). The outer edge of the viscous superlayer in a TNTI is defined as an enstrophy isosurface of $\omega^2 = 0$. This holds true in a TNTI as the free stream is irrotational. The lack of rotational fluid in the free stream is also the condition that forces the vorticity stretching term to be insignificant in the viscous superlayer, thereby defining the important role of viscosity in the outer regions of the TNTI. For a TTI, rotational flow is readily available on both sides of the boundary, therefore lifting the constraint that ensures enstrophy production through vorticity stretching decays to zero at the wake boundary. We therefore question what is the role of viscosity in a TTI? figures 4, 5(*a*) and 5(*b*) depict the interface-conditioned behaviour of the vorticity stretching and viscous diffusion terms for all of the runs conducted in the present experimental campaign. It is important to highlight the behaviour of run 1a, which is our closest approximation to a TNTI. Figure 6(*a*) isolates run 1a and provides a zoomed-in look at the interfacial region.
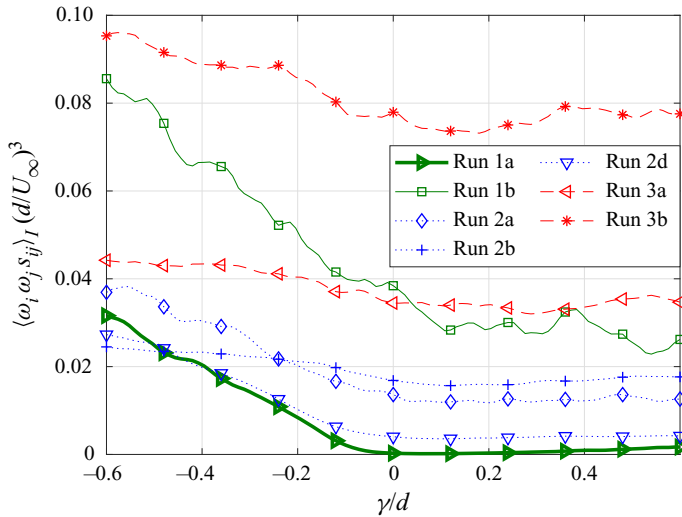
Figure 4. The inertial term of the enstrophy budget equation as a function of normal distance away from the interface.

The TNTI that this run captures reproduces results that are remarkably similar to the TNTI results found in the literature, notably from DNS of the governing Navier–Stokes equations (e.g. Taveira & da Silva 2014; Watanabe *et al.* 2014; Silva *et al.* 2018). The vanishingly small level of enstrophy production on the background/free-stream side of the wake boundary ($\gamma > 0$) is clearly evident with respect to both the vorticity stretching as well the viscous diffusion terms. With added background turbulence, the vorticity stretching term is no longer constrained to be zero at $\gamma = 0$ and is free to contribute to enstrophy production throughout the entire thickness of the interface. All runs exposed to background turbulence see an increase in enstrophy production across the whole of the interface. Runs in group 3 especially see significantly greater production through the vorticity stretching term, which should be expected considering the extreme conditions in the background turbulence that are present for these runs.

In order to ascertain the role of viscosity, the viscous diffusion term has been plotted for groups 1 and 2 and for group 3 in figures 5(*a*) and 5(*b*), respectively. With respect to the no-grid case, the behaviour observed in DNS studies, including the characteristic peak in production near the outer edge of the interface (viscous superlayer), is reproduced, e.g. da Silva *et al.* (2014). Viscous diffusion acts as a source of enstrophy near $\gamma = 0$ but it quickly reverts to a sink for small values of $\gamma < 0$ (within the wake). The viscous diffusion term acts in a similar manner to the no-grid case for runs in groups 1 and 2 with minimal activity in the free stream followed by source behaviour at the outer edge of the interface. All cases with background turbulence exhibit increased statistical noise which may be expected since fewer usable snapshots are captured (i.e. where the interface spans the entirety of the field of view). However, even with the increased noise the underlying behaviour can be established for groups 1 and 2. This is not the case for runs that lie in group 3 where all of the similarity to the no-grid case is lost. The level of noise is also greater as the characteristic production peak is no longer distinctly visible. Most importantly, the magnitude of the viscous diffusion term is insignificant when compared with the amount of enstrophy produced through vorticity stretching for cases with free-stream turbulence (both terms are plotted in figure 6(*b*) for a few cases).
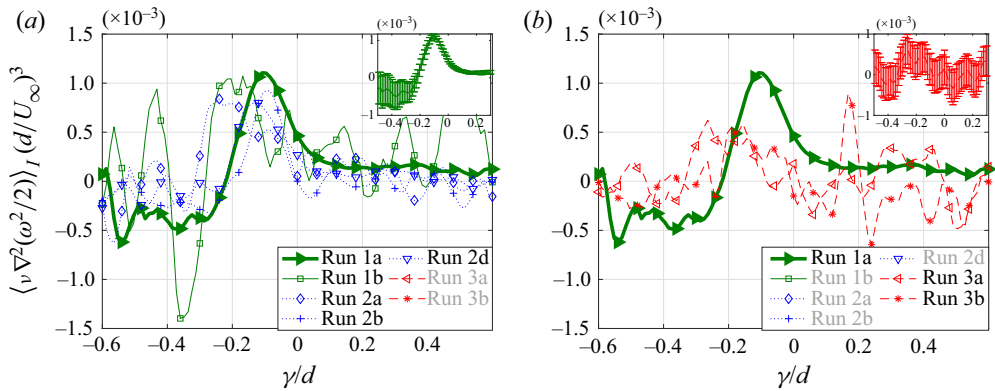
Figure 5. The interface-conditioned plot of the viscous diffusion term of the enstrophy budget equation for cases in (*a*) groups 1 and 2, and (*b*) group 3. The insets display 95 % confidence intervals for the no-grid (*a*) and run 3a (*b*) cases. Labels have been omitted as they remain the same as the main set of axes.
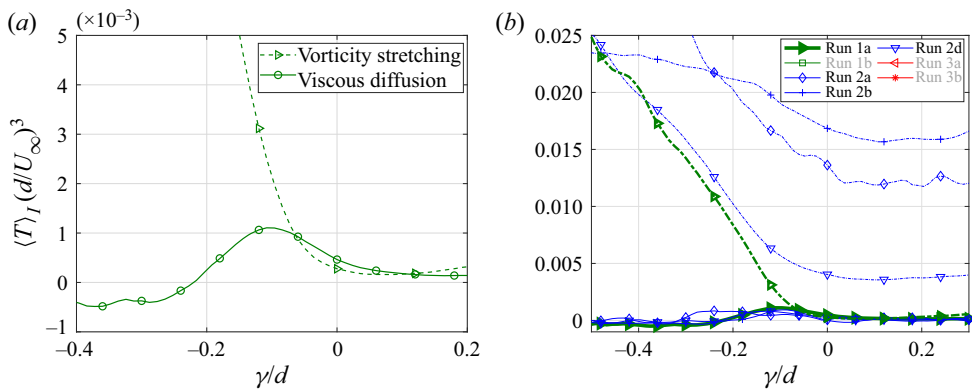

Figure 6. Behaviour of the terms of the enstrophy budget equation (T) for (*a*) the no-grid case and (*b*) zoomed-in plot of both terms for a few cases with background turbulence.

Our results show that the role of viscosity in terms of the relative strength of the viscous diffusion term is much reduced in a TTI, to the point of insignificance. Kankanwadi & Buxton (2020) clearly demonstrated the existence of an interfacial layer between the background turbulence and that within the wake, which manifests itself as a discontinuity/jump in enstrophy. However, viscous action is no longer the only mechanism through which enstrophy may be produced in the outer regions of the interface. The availability of turbulent vorticity/strain rate uncages the vorticity stretching term which thereby acts as the main producer of the enstrophy that yields this discontinuity, and allows it to participate in the turbulent/turbulent entrainment process. This has implications for the arguments pertaining to the scaling of the thickness of the TTI, since there is no longer a relevant physical argument (as there is for a TNTI) to suggest that a TTI's thickness scales with the viscous Kolmogorov length scale. Further, it has connotations for numerical modelling of turbulent/turbulent entrainment since it is inertial vorticity stretching, which is an intermittent quantity, and not viscous diffusion that is active within the TTI.

Previous work (Cimarelli *et al.* 2015; Buxton *et al.* 2019; Kankanwadi & Buxton 2020) showed that the presence of a turbulent interface introduces a strong, small-scale
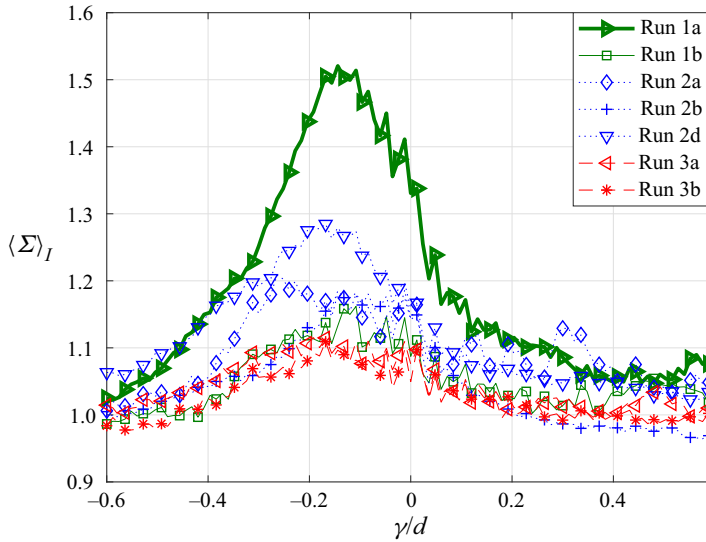
Figure 7. Interface-conditioned plot of anisotropy in the vicinity of the interface.

anisotropy into the flow; enhancing strain rates in the interface-normal direction somewhat analogously to a wall in wall-bounded turbulence. This is further verified in this paper in figure 7. Here, interface-conditioned anisotropy has been calculated two dimensionally in the transverse (y–z) plane considering only the v and w velocity components. Mathematically, we define the anisotropy in the context of a ratio of interface-normal velocity gradient to interface-parallel velocity gradient magnitudes, $\langle \Sigma \rangle_I = \langle (\mathrm{d}u'_\gamma/\mathrm{d}\gamma)^2 \rangle / \langle (\mathrm{d}u'_\xi/\mathrm{d}\xi)^2 \rangle$. Here, γ and ξ represent interface-normal and interface-parallel coordinate directions, with u'_γ and u'_ξ representing fluctuating velocity components in this interface coordinate system. Far away from the interface $\langle \Sigma \rangle_I$ is close to unity (i.e. isotropy) but a peak in this anisotropy metric in the vicinity of the wake boundary denotes disproportionately larger velocity gradients (strain rates) in the interface-normal direction within the TTI. These enhanced strain rates offer a potential explanation for the enhanced enstrophy production, and, hence, enstrophy jump, in TTIs. However, enstrophy production through vorticity stretching depends not only on the magnitude of the strain-rate tensor and vorticity vector but also the alignment between the two. If the vorticity is somehow more 'organised' in the wake than the free stream, i.e. exploiting this enhanced interface-normal strain rate and more efficiently aligning itself with the extensive strain rate that yields $\omega_i s_{ij} \omega_j > 0$, then enhanced enstrophy production will be found on the wake side of the TTI. Such an argument also offers an explanation for the conditional mean enstrophy jump occurring even for group 3 cases, in which the intensity of the turbulence in the background is greater than in the wake.

We test this hypothesis by examining the relative contribution of the strain rate normal to the interface to the overall enstrophy production $\omega_i s_{ij} \omega_j$. We choose to do this by deconstructing the vorticity stretching term using the Betchov decomposition (Betchov 1956), $\omega_i s_{ij} \omega_j = \omega^2 s_i (\hat{\boldsymbol{e}}_i \cdot \hat{\boldsymbol{\omega}})^2$, where s_{ij} and s_i are the strain-rate tensor and the eigenvalues of the strain-rate tensor, respectively. This decomposition illustrates that it is not simply the magnitude of the strain-rate tensor (and vorticity), but also the alignment between the strain-rate eigenvectors and the vorticity vector that determines the level of enstrophy
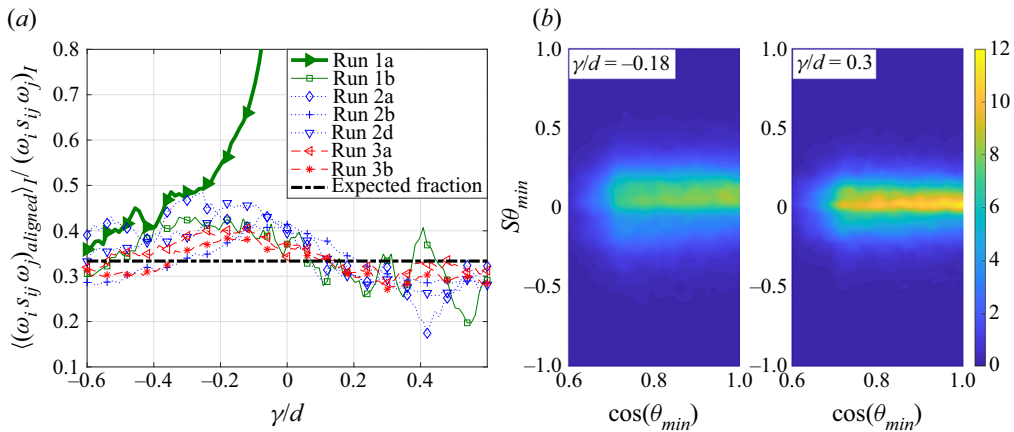
(*a*)

(*b*)

Figure 8. (*a*) Interface-conditioned plot of the interface-normal aligned contribution of the overall vorticity stretching term. Note that the black dot-dashed line represents the expected fraction in isotropic turbulence. (*b*) Joint PDF of the most aligned strain-rate eigenvalue and cosine of the alignment angle between said strain rate and the interface-normal direction for run 2d.

production through vorticity stretching ($\widehat{e_i}$ and $\hat{\omega}$ represent unit vectors pointing in the direction of the strain-rate eigenvectors and the vorticity vector, respectively).

We now examine the contribution to $\omega_i s_{ij} \omega_j$ from the principal strain rate that is most aligned with the interface-normal vector that was extracted $\hat{\gamma}$. Prior to examining the results, it is important at this stage to address a couple of assumptions made during the analysis. The current analysis is independent of the particular orientation of the strain-rate eigenvectors, i.e.no distinction is made between vectors pointing in a particular direction or a direction rotated by π. Mathematically, the alignment angle is redefined as $\theta_i = \min(\theta_i, \pi - \theta_i)$. Furthermore, it is important to note that the interface is assumed to be two dimensional in the cross-stream plane (i.e. the streamwise component of $\hat{\gamma}$ is constrained to be equal to zero). Returning to the analysis, in isotropic turbulence the contribution of the vorticity stretching terms corresponding to the three principal strain directions that have been decomposed through the Betchov decomposition should be all of equal magnitude. However, this does not hold true in the vicinity of the interface due to the small-scale anisotropy created by the presence of the interface. Figure 8(*a*) plots the fraction of enstrophy produced through the term most aligned with the interface-normal direction ($\max\{|\hat{e_i} \cdot \hat{\gamma}|\}$), with respect to the total enstrophy production through vorticity stretching. Mathematically, this is represented as $\omega^2 s_{aligned}(\hat{e}_{aligned} \cdot \hat{\omega})^2 / \omega_i s_{ij} \omega_j$. Similarly to the previous plots, this figure shows this behaviour as a function of distance normal to the interface γ. It should be noted that only the values inside the wake have been plotted for the no-grid case, since the vorticity stretching term is negligible in the free stream for this case. It is clear to see from the figure that on the wake side of the interface the aligned contribution is significantly larger than the expected 1/3 ratio, thereby supporting the initial hypothesis that vorticity inside the wake is more 'organised' allowing for increased enstrophy production.

Elsinga & da Silva (2019) examine the TNTI in a data set obtained using DNS of a planar jet. They show that at the irrotational boundary there is preferential alignment of the most compressive strain-rate eigenvevector and the interface-normal direction. Whilst, at first sight this seems a contradiction to increased aligned contribution to interial enstrophy production that is observed here, it may be possible to explain this result. Elsinga &

da Silva (2019) observe the preferential alignment of the most compressive strain-rate eignevector and the interface-normal direction at the irrotational boundary itself ($\gamma = 0$). This preferential alignment of the most compressive eigenvector is seen to decrease at positions further into the wake side of the interface, as the alignment of the most stretching term is seen to increase. In our study the observed peak of aligned contribution occurs in a region that is offset into the wake side of the boundary ($\gamma \lesssim 0$). The peak in the aligned contribution observed in figure 8(*a*) occurs approximately between $0.2d$ to $0.3d$ into the wake side of the interface. This translates to $-0.7\lambda_{no\,grid}$ and $-1.1\lambda_{no\,grid}$, respectively, where $\lambda_{no\,grid}$ is the Taylor length scale calculated for the no-grid case. Note that the Taylor scale is calculated using the following relation, $\lambda_{no\,grid} = \sqrt{10\nu k/\varepsilon}$, where k is the turbulent kinetic energy and ε is the dissipation rate. Elsinga & da Silva (2019) explain that vortex stretching maintains a large magnitude in this region, which lies in the turbulent sublayer. Furthermore, da Silva & dos Reis (2011), who examine coherent structures at the TNTI, explain that large-scale vortical structures that scale with the Taylor microscale exist in the interfacial region and are in-turn responsible for producing the vorticity jump. Therefore, it is likely that the aligned peak witnessed in this study is a by-product of the large-scale vortical structures highlighted by da Silva & dos Reis (2011). An alternative explanation may be to do with the role of viscosity. Results in this chapter have shown the role of viscosity is not significant in a TTI. In a TNTI it may be possible that viscosity acts as a damper for the turbulent strain at the irrotational boundary, which may favour compressive strain rate rather than extensive strain rate. With the subdued role of viscosity in the TTI, such a mechanism would not apply. In the no-grid case the sharp rise in the aligned contribution occurs approximately 1λ into the wake side of the interface. This metric however continues to rise, although it is a result of the insignificant magnitude of the vorticity stretching term near the irrotational boundary, producing large ratios.

Lastly, the underlying actors responsible for the increased aligned contribution to enstrophy production are visually depicted in figure 8(*b*). Plotted is the joint probability density function (PDF) of the cosine of the most aligned angle between principal strain rate and the interface-normal direction, $\cos(\theta_{min}) = \max\{|\hat{\boldsymbol{e}}_i \cdot \hat{\boldsymbol{\gamma}}|\}$ as well as the corresponding eigenvalue ($s_{\theta_{min}}$). A positive value of $s_{\theta_{min}}$ corresponds to vortex stretching (extension), whereas $s_{\theta_{min}} < 0$ reflects compression. In the interest of brevity only a single joint PDF of run 2d has been shown. However, this is a typical example of what can be observed for runs subjected to free-stream turbulence. In the wake side of the interface a clear bias can be seen toward extension across the range of alignment angles, thereby boosting enstrophy production in this region ($\omega_i s_{ij} \omega_j > 0$). Such skewed behaviour is no longer present on the free-stream side of the interface. Whilst a slight bias towards extension still exists as is expected for homogeneous turbulence (Taylor 1938), it is not comparable to what is seen on the wake side of the interface. We thus conclude that introduction of the small-sale anisotropy in the TTI coupled to the preferential alignment of the vorticity vector with the interface-normal direction is responsible for producing the enstrophy jump observed in a TTI.

5. Conclusions

The TTI was examined in detail through interface-conditioned statistics of the enstrophy budget terms. The role of viscosity is known to be of critical importance in the TNTI, as it is the sole mechanism by which enstrophy is imparted to the background fluid across a TNTI. However, with rotational fluid available in the free-stream side of a TTI, the vorticity stretching term is free to contribute to enstrophy production throughout the entire thickness of the interface. Results showed that the magnitude of enstrophy production

through the vorticity stretching term dwarfed that of the viscous term throughout the entire interface and, therefore, it is possible to conclude that in a TTI the role of viscosity is reduced to insignificance as the vorticity stretching term takes over responsibilities for the enstrophy production. Furthermore, similarly to a wall in wall-bounded turbulence, the TTI acts to enhance strain rates in the interface-normal direction close to the boundary. Finally, decomposing the vorticity stretching term into three terms corresponding to the three principal strain directions highlighted that the component most aligned to the interface-normal direction contributes the largest share of enstrophy production on the wake side of the interface. This is indicative of better 'organised' vorticity on the wake side, thereby taking advantage of the strong interface-normal strain rates to produce the enstrophy jump observed in a TTI. These results have important implications with regards to modelling entrainment behaviour in a turbulent environment as the role of vorticity stretching is instrumental in the entrainment process, something typically neglected when only considering entrainment from a non-turbulent background.

The results presented in this paper lead to open questions regarding the phenomenology of a TTI. The structure of a TNTI is well known, as there are distinct layers in which, respectively, viscous and inertial processes dominate the flow physics. For example, it is possible to claim that the viscous superlayer is bounded between the irrotational boundary and the location where the inertial vorticity stretching term produces a larger share of enstrophy than the viscous term (Taveira & da Silva 2014). However, these bounds lack any physical relevance when applied to the TTI. The internal structure of the TTI must therefore be further investigated. It is interesting to note that even with turbulence available in the background, the viscous diffusion term for groups 1 and 2 produces a production peak similar to the no-grid case. Hence, it is possible to raise the question, is this a remnant of a defunct viscous superlayer? Additionally, with a diminished role of viscosity, there is also no longer a relevant physical argument supporting the scaling of the thickness of the TTI with the Kolmogorov length scale. The scaling of the TTI is therefore also an open question.

Lastly, it should be noted that by considering the far wake (i.e. a fully developed turbulent shear flow), it is assumed that the generality of the study is increased, with the analysis being more applicable to other flows, such as jets and even boundary layers (Silva *et al.* 2018; Watanabe, Zhang & Nagata 2018). Whilst it is not possible to claim any universality, since that would require experiments conducted over a large range of Reynolds numbers using several flow types, the results are robust within the extensive parametric envelope that was investigated. Free-stream turbulence conditions that were considered had length scales both larger and smaller than the wake-generating object as well as intensities smaller and larger than within the wake.

Declaration of interests. The authors report no conflict of interest.

Author ORCIDs.

Krishna S. Kankanwadi https://orcid.org/0000-0003-4888-5947;

Oliver R.H. Buxton https://orcid.org/0000-0002-8997-2986.

REFERENCES

ATREYA, S.K., WONG, M.H., OWEN, T.C., MAHAFFY, P.R., NIEMANN, H.B., DE PATER, I., DROSSART, P. & ENCRENAZ, T. 1999 A comparison of the atmospheres of Jupiter and Saturn: deep atmospheric composition, cloud structure, vertical mixing, and origin. *Planet. Space Sci.* **47** (10), 1243–1262.

BETCHOV, R. 1956 An inequality concerning the production of vorticity in isotropic turbulence. *J. Fluid Mech.* **1** (5), 497–504.

BISSET, D.K., HUNT, J.C.R. & ROGERS, M.M. 2002 The turbulent/non-turbulent interface bounding a far wake. *J. Fluid Mech.* **451**, 383–410.

BUXTON, O.R.H., BREDA, M. & DHALL, K. 2019 Importance of small-scale anisotropy in the turbulent/nonturbulent interface region of turbulent free shear flows. *Phys. Rev. Fluids* **4** (3), 034603.

CHING, C.Y., FERNANDO, H.J.S. & ROBLES, A. 1995 Breakdown of line plumes in turbulent environments. *J. Geophys. Res.: Oceans* **100** (C3), 4707–4713.

CIMARELLI, A., COCCONI, G., FROHNAPFEL, B. & DE ANGELIS, E. 2015 Spectral enstrophy budget in a shear-less flow with turbulent/non-turbulent interface. *Phys. Fluids* **27** (12), 125106.

CORRSIN, S. & KISTLER, A.L. 1955 Free-stream boundaries of turbulent flows. *NACA technical report* 1244.

EAMES, I., JONSSON, C. & JOHNSON, P.B. 2011 The growth of a cylinder wake in turbulent flow. *J. Turbul.* **12**, 39.

ELSINGA, G.E. & DA SILVA, C.B. 2019 How the turbulent/non-turbulent interface is different from internal turbulence. *J. Fluid Mech.* **866**, 216–238.

GANAPATHISUBRAMANI, B., LAKSHMINARASIMHAN, K. & CLEMENS, N.T. 2007 Determination of complete velocity gradient tensor by using cinematographic stereoscopic PIV in a turbulent jet. *Exp. Fluids* **42**, 923–939.

GASKIN, S.J., MCKERNAN, M. & XUE, F. 2004 The effect of background turbulence on jet entrainment: an experimental study of a plane jet in a shallow coflow. *J. Hydraul Res.* **42** (5), 533–542.

HOLZNER, M., LIBERZON, A., NIKITIN, N., KINZELBACH, W. & TSINOBER, A. 2007 Small-scale aspects of flows in proximity of the turbulent/nonturbulent interface. *Phys. Fluids* **19** (7), 071702.

HUNT, J.C.R., EAMES, I., WESTERWEEL, J., DAVIDSON, P.A., VOROPAYEV, S., FERNANDO, J. & BRAZA, M. 2010 Thin shear layers – the key to turbulence structure? *J. Hydro-Environ. Res.* **4** (2), 75–82. Special Issue II on Shallow Flows - Dedicated to Prof. Gerhard H. Jirka.

ISHIHARA, T., KANEDA, Y. & HUNT, J.C.R. 2013 Thin shear layers in high Reynolds number turbulence - DNS results. *Flow Turbul. Combust.* **91** (4), 895–929.

KANKANWADI, K.S. & BUXTON, O.R.H. 2020 Turbulent entrainment into a cylinder wake from a turbulent background. *J. Fluid Mech.* **905**, A35.

DE ROOY, W.C., BECHTOLD, P., FRÖHLICH, K., HOHENEGGER, C., JONKER, H., MIRONOV, D., PIER SIEBESMA, A., TEIXEIRA, J. & YANO, J.-I. 2013 Entrainment and detrainment in cumulus convection: an overview. *Q. J. R. Meteorol. Soc.* **139** (670), 1–19.

DA SILVA, C.B., HUNT, J.C.R., EAMES, I. & WESTERWEEL, J. 2014 Interfacial layers between regions of different turbulence intensity. *Annu. Rev. Fluid Mech.* **46** (1), 567–590.

DE SILVA, C.M., PHILIP, J. & MARUSIC, I. 2013 Minimization of divergence error in volumetric velocity measurements and implications for turbulence statistics. *Exp. Fluids* **54**, 1557.

DA SILVA, C.B. & DOS REIS, R.J.N. 2011 The role of coherent vortices near the turbulent/non-turbulent interface in a planar jet. *Phil. Trans. R. Soc.* A*: Math. Phys. Engng Sci.* **369** (1937), 738–753.

SILVA, T.S., ZECCHETTO, M. & DA SILVA, C.B. 2018 The scaling of the turbulent/non-turbulent interface at high Reynolds numbers. *J. Fluid Mech.* **843**, 156–179.

TAVEIRA, R.R. & DA SILVA, C.B. 2014 Characteristics of the viscous superlayer in shear free turbulence and in planar turbulent jets. *Phys. Fluids* **26** (2), 021702.

TAYLOR, G.I. 1938 Production and dissipation of vorticity in a turbulent fluid. *Proc. R. Soc. Lond. Ser.* A - *Math. Phys. Sci.* **164** (916), 15–23.

VAN REEUWIJK, M. & HOLZNER, M. 2013 The turbulence boundary of a temporal jet. *J. Fluid Mech.* **739**, 254–275. arXiv:1304.0476.

WATANABE, T., SAKAI, Y., NAGATA, K., ITO, Y. & HAYASE, T. 2014 Vortex stretching and compression near the turbulent/non-turbulent interface in a planar jet. *J. Fluid Mech.* **758**, 754–785.

WATANABE, T., ZHANG, X. & NAGATA, K. 2018 Turbulent/non-turbulent interfaces detected in DNS of incompressible turbulent boundary layers. *Phys. Fluids* **30** (3), 035102.

WESTERWEEL, J., FUKUSHIMA, C., PEDERSEN, J. & HUNT, J.C.R. 2005 Mechanics of the turbulent-nonturbulent interface of a jet. *Phys. Rev. Lett.* **95** (17), 199902.